Near-infrared spectroscopy of $LiNH_3$: First observation of the electronic spectrum

Luigi Varriale,[1] Nitika Bhalla,[1] Nicola M.Tonge,[1] Andrew M. Ellis,[1,a)] and Timothy G. Wright[2,b)]
[1]*Department of Chemistry, University of Leicester, University Road, Leicester LE1 7RH, United Kingdom*
[2]*School of Chemistry, University of Nottingham, University Park, Nottingham NG7 2RD, United Kingdom*

(Received 10 February 2011; accepted 7 March 2011; published online 23 March 2011)

Electronic spectra of $LiNH_3$ and its partially and fully deuterated analogues are reported for the first time. The spectra have been recorded in the near-infrared and are consistent with two electronic transitions in close proximity, the $\tilde{A}^2E-\tilde{X}^2A_1$ and $\tilde{B}^2A_1-\tilde{X}^2A_1$ systems. Vibrational structure is seen in both systems, with the Li–N–H bending vibration (ν_6) dominant in the $\tilde{A}^2E-\tilde{X}^2A_1$ system and the Li–N stretch (ν_3) in the $\tilde{B}^2A_1-\tilde{X}^2A_1$ system. The prominence of the 6_0^1 band in the $\tilde{A}^2E-\tilde{X}^2A_1$ spectrum is attributed to Herzberg–Teller coupling. The proximity of the $\tilde{B}^2A_1$ state, which lies a little more than 200 cm^{-1} above the $\tilde{A}^2E$ state, is likely to be the primary contributor to this strong vibronic coupling. © *2011 American Institute of Physics*. [doi:10.1063/1.3570824]

I. INTRODUCTION

All of the alkali metals dissolve in liquid ammonia.[1] The resulting solutions have properties that depend strongly on the alkali/ammonia mole ratio. At high alkali concentrations, the solutions have a shiny metallic appearance and show high electrical conductivities consistent with metallicliike behavior. In contrast, dilute solutions of the alkali in liquid ammonia are electrically insulating and show a deep blue color. The electrical and optical properties of these solutions have long been attributed to the valence electron of the alkali metal, which can detach from the atom and enter the liquid ammonia to form a solvated electron when the solution is sufficiently dilute. It is transitions of these solvated electrons that are responsible for the color of the solution and the absorption wavelength is determined by the precise environment in which the electron is located, which in turn depends upon the alkali/ammonia ratio.

The study of clusters of alkali metal atoms with ammonia molecules in the gas phase provides a means of probing the impact of the solute/solvent ratio on the electronic properties in a system of finite size. The latter is particularly valuable because small complexes are, in principle, amenable to high quality *ab initio* calculations, which can then be compared directly with experimental findings.[2] The smallest, and ostensibly the simplest, alkali-ammonia cluster is $LiNH_3$. Any attempt to understand small alkali-ammonia clusters, and to extrapolate their properties as a function of cluster size, should include this most fundamental complex. However, the only previous experimental studies of $LiNH_3$ have been carried out in solid argon matrices.[3,4] Using infrared spectroscopy, the fundamental frequencies of several vibrational modes of $LiNH_3$ and its deuterated analogues were determined.

Here we report the first observation of the electronic spectrum of $LiNH_3$. This is part of a series of investigations of alkali/ammonia complexes and complements our earlier spectroscopic work on the ground electronic states of these complexes.[5,6] The only previous study of the electronic spectroscopy of $Li(NH_3)_n$ complexes was a recent investigation of $Li(NH_3)_4$ originating from our laboratory, which employed photodissociation spectroscopy.[7] Very recently, this work has been complemented by a velocity map imaging study to explore the photodissociation dynamics in the first excited electronic state of $Li(NH_3)_4$.[8] More extensive spectroscopic work has been carried out on small $Na(NH_3)_n$ complexes and the first such study was reported by Nitsch and co-workers,[9] who successfully obtained spectra for $NaNH_3$. This and subsequent work by Schulz and co-workers,[10] and also by Rodham and Blake,[11] on both $NaNH_3$ and $NaND_3$, has yielded resolved vibrational structure. Extension to larger complexes, with up to $n = 6$, was achieved by Brockhaus and co-workers,[12] but the spectra were broad and unresolved, unlike that of $NaNH_3$. The transitions observed for the $n = 1-6$ complexes all occur in the near-infrared and correlate asymptotically with the $3p \leftarrow 3s$ transition of atomic sodium. One of the defining features of the $NaNH_3$ spectrum is strong vibronic coupling, as evinced by intense bands originating from excitation of a low frequency degenerate bending vibration, whose observation should be symmetry forbidden in the Franck–Condon limit for a molecule of C_{3v} symmetry. The origin of this vibronic coupling, whether a Jahn–Teller effect or Herzberg–Teller coupling, or indeed a combination of the two, has not been determined. Predictions of the vertical transition energies to low-lying excited electronic states of both $LiNH_3$ and $NaNH_3$ have recently been published,[13,14] but neither geometries nor vibrational frequencies were reported for these complexes in their excited electronic states.

Electronic spectra of both $LiNH_3$ and its partially- and fully-deuterated analogues are presented in the current study. These spectra were successfully obtained using

a)Author to whom correspondence should be addressed. Electronic mail: andrew.ellis@le.ac.uk. Telephone +44 (0)116 252 2138; Fax +44 (0)116 252 3789.
b)Electronic mail: tim.wright@nottingham.ac.uk. Telephone +44 (0)115 846 7076; Fax +44 (0)115 951 3562.

both two-color resonance-enhanced multiphoton ionization (REMPI) and a photodepletion technique. The spectra show a number of features, which appear to be vibrational or vibronic in origin, and their assignment is discussed in the light of results obtained for partially- and fully-deuterated molecules.

II. EXPERIMENTAL

The experimental procedure and apparatus employed were similar to that described in previous studies in our laboratory.[5–7] Briefly, $LiNH_3$ complexes were produced by laser ablation of a solid lithium target in the presence of gaseous NH_3 and the resulting mixture was expanded into vacuum to form a supersonic jet. The central portion of the jet was extracted by a skimmer and the resulting molecular beam passed into the source region of a time-of-flight mass spectrometer. To gain some information on the species formed during the expansion, single-photon ionization in the near-UV was employed using the output from a pulsed dye laser. The dominant ions present were $LiNH_3^+$ and $Li(NH_3)_4^+$, although significant quantities of other $Li(NH_3)_n^+$ ions were also observed.

To record optical spectra, the output from a LaserVision optical parametric oscillator/amplifier (OPO/A) was employed. This system was pumped by the output from an injection-seeded Nd:YAG laser (Surelite II-10), although the injection seeder was not essential for the experiments described here, since it did not affect the observable resolution. Since all of the spectra were recorded in the near-infrared, only the OPO part of the OPO/A system was used. This gave a wavelength-tuneable output capable of pulse energies of up to 15 mJ, although the pulse energy incident on the molecular beam was typically 0.5 mJ. The beam from the OPO was gently focused into the source region of the mass spectrometer and aligned such that it spatially overlapped the UV laser beam. The delay between the firing of the two laser pulses was controlled using a delay generator.

Both two-color $(1+1')$ REMPI and photodepletion spectroscopy were used to record spectra, with the latter yielding much higher quality spectra, as detailed later.

Ammonia was obtained from a standard liquid ammonia cylinder (BOC Gases, 99% purity) and was used without purification. To assist with spectral assignments some experiments were also carried out using ND_3 (Sigma Aldrich, 99% D).

III. COMPUTATIONAL DETAILS

Ab initio calculations on $LiNH_3$ have been carried out in support of the experimental work. We have previously reported *ab initio* calculations on the ground electronic state of $LiNH_3$ at levels up to and including UCCSD(T) with an aug-cc-pVQZ basis set.[15] These high level calculations were used to predict both the vibrational frequencies and the Li–N bond dissociation energy. The aims of the new calculations were twofold: (1) to predict vibrational isotopic shifts for the ground state and (2) to explore the low-lying excited electronic states. For the ground state calculations, UMP2/6–311++G** calculations were initially performed using the GAUSSIAN 03 program.[16] Spin contamination was found to be negligible, as shown by the calculated value of $<S^2> = 0.7501$. The geometry was optimized and harmonic vibrational frequencies calculated at the potential energy minimum. In addition, RCCSD(T) calculations were also performed, with again both geometry optimization and harmonic frequency calculations being undertaken: these calculations employed MOLPRO 2008.[17] For N and H, standard Dunning aug-cc-pVTZ basis sets were employed. For Li, the cc-pVTZ basis set was extended by adding a single set of diffuse *s*, *p,* and *d* basis functions, extrapolated in an even-tempered fashion from the existing basis functions with the smallest exponents.

Hashimoto and Daigoku have recently computed the vertical transition energies to low-lying electronic states of $LiNH_3$ using multireference calculations (MRCI-SD).[14] In the current study, we undertook a series of CASSCF and CASSCF+MRCI calculations. For the CASSCF calculations, the basis set was as described above for the RCCSD(T) calculations, while for the CASSCF+MRCI calculations, we employed aug-cc-pVDZ basis sets for N and H and the cc-pVDZ basis set for Li. MOLPRO 2008 (Ref. 17) was used for all of the CASSCF and CASSCF+MRCI calculations. The aim was to obtain excitation energies, as well as geometries and vibrational frequencies for the ground and excited states. These calculations proved to be far from straightforward, especially with regard to calculation of the vibrational frequencies.

Initially, the strategy adopted was to use state-averaged CASSCF, with the triple-ζ basis set mentioned above. The four lowest energy roots arising from the interaction of Li with NH_3 were considered, where Li had the unpaired electron in either the $2s$ or $2p$ orbitals. As will be discussed in more detail later, these four roots correspond to the $\tilde{X}^2A_1$, $\tilde{A}^2E$, and $\tilde{B}^2A_1$ states, where C_{3v} symmetry is assumed in these labels. Both the Li and N $1s$ orbitals were kept doubly occupied during this procedure, although their coefficients were allowed to vary. Analytic gradients were employed for optimizing the geometry, by using the RS2 procedure within MOLPRO,[17] but not allowing any excitations; however, the second derivatives were calculated numerically and this required convergence at all displaced geometries. Unfortunately, even with small step sizes in the numerical gradient calculation, the vibrational frequencies for the ^2E state came out with imaginary frequencies and severe nondegeneracy of the vibrational modes with nominal *e* symmetry (although the geometries and the energies of the two components of this state were essentially identical). Indeed, the two components of the ^2E state, calculated separately, did not give vibrational frequencies in even approximate agreement with each other. Even for the nondegenerate $\tilde{X}$ and $\tilde{B}$ states, nondegeneracy in the *e* vibrations was observed, even when C_{3v} symmetry was imposed. Similar results were obtained when each root was considered separately in single-reference CISD calculations.

Further calculations were then undertaken where multireference CI was performed on the CASSCF wavefunctions obtained with the double-ζ basis set. It was found that the values obtained for the $\tilde{X}$ state were now in good agreement with

TABLE I. Calculated equilibrium parameters for $LiNH_3$ and $LiNH_3^+$.

	$LiNH_3$				$LiNH_3^+$
	RCCSD(T)	CASSCF + MRCI			(R)CCSD(T)
Parameter	$\tilde{X}^2A_1$	$\tilde{X}^2A_1$	$\tilde{A}^2E$	$\tilde{B}^2A_1$	$\tilde{X}\ ^1A_1$ [a]
R_{LiN}/ Å	2.022	2.042	2.043	1.966	1.985
R_{NH}/ Å	1.018	1.021	1.018	1.031	1.019
θ_{LiNH} / °	112.4	112.1	112.2	114.4	113.9
T_e / cm^{-1}	0	0	11463	11806	34535 [b]

[a]Note that these parameters for the cation agree closely with those described in Ref. 15, which were also calculated using UCCSD(T) methodology.
[b]This is the first ionization energy of $LiNH_3$ excluding zero point energy effects. Inclusion of zero point energy corrections in the neutral molecule and cation gives an adiabatic ionization energy of 34845 cm^{-1} (4.32 eV).

those from the RCCSD(T)/aug-cc-pVTZ calculations. There were, however, still nondegenerate and imaginary vibrational frequencies for the $\tilde{A}^2E$ state. As a consequence, we have been unable to obtain vibrational frequencies for the ^2E state. The same set of calculations did, however, yield a full set of real vibrational frequencies for the $\tilde{X}^2A_1$ state and the $\tilde{B}^2A_1$ states, and which also showed the expected degeneracies, and the results of this latter set of calculations are discussed below.

IV. RESULTS AND DISCUSSION

A. *Ab initio* calculations

We begin with a discussion of the results from the *ab initio* calculations, since these provide information that has proved to be important in achieving a spectral assignment. The minimum energy structures in all three electronic states of $LiNH_3$, derived from CASSCF+MRCI calculations, are summarized in Table I. For comparison purposes, we also include structures for the ground states of both $LiNH_3$ and $LiNH_3^+$ obtained from CCSD(T) calculations. Caution is needed in interpreting the theoretical findings for the $\tilde{A}^2E$ state since, as mentioned earlier, some imaginary vibrational frequencies were calculated for the two components of this state. Nevertheless, in all of the neutral and ionic states the minimum energy structure was found to correspond to C_{3v} symmetry. According to the calculations the minima of the $\tilde{A}^2E$ and $\tilde{B}^2A_1$ states are separated by <350 cm^{-1}, a point of significance which will be encountered again later. It should also be noted that the calculated adiabatic ionization energy obtained from these calculations, 4.32 eV (inclusive of zero-point vibrational energy), is in excellent agreement with the experimentally determined value of 4.339 ± 0.003 eV.[18]

An important take-home message from these calculations is that the change in structure in moving from the $\tilde{X}^2A_1$ state to the $\tilde{A}^2E$ state is small, whereas excitation to the $\tilde{B}^2A_1$ state leads to a much more significant change in structure, specifically in the Li–N bond length. Indeed the Li–N bond is found to be even shorter in the $\tilde{B}^2A_1$ state than in the cation, which would not be expected if the unpaired electron was simply a nonbonding electron. In fact in the limit of a nonbonding electron the $\tilde{A}^2E$ state should possess the shortest bond, since the orientation of the unpaired electron, which would now lie in orbitals that correlate with the $2p_{x,y}$ orbital pair on the Li atom, would expose the N atom to an increase in effective positive charge on the Li atom. By way of contrast, in the $\tilde{B}^2A_1$ state the Li–N bond length would be expected to be longer than that in the $\tilde{X}^2A_1$ state, since increased electron–electron repulsion would arise from the unpaired electron residing in what is approximately a $2p_z$ orbital pointing directly at the N atom. This simple electrostatic picture is clearly deficient for $LiNH_3$ and suggests that the unpaired electron has a significant *covalent* bonding role, particularly in the $\tilde{B}^2A_1$ state.

Under C_{3v} symmetry $LiNH_3$ will have six distinct vibrational frequencies and Table II shows the *ab initio* predictions alongside experimental values for the ground electronic state of $LiNH_3$ derived from IR matrix isolation spectroscopy.[3,4] Although the argon matrix will perturb the vibrations, the effect on the vibrational frequencies is normally small and the shifts relative to the gas phase tend to be a few cm^{-1} at most. Confirmation that the matrix IR assignments are reasonable is provided by the relatively good agreement with our *ab initio* vibrational frequencies. The only exception to this statement is for mode ν_3, the Li–N stretch, where a significant discrepancy between theory and experiment is seen. The same conclusion has been reached in a recent DFT study of MNH_3 complexes,[19] where M = Li–Fr, and therefore the matrix assignment of the Li–N stretching frequency in $LiNH_3$ looks to be erroneous. Also, the corresponding data for $LiND_3$ are shown in Table II. The effect of deuteration in the matrix experiments is faithfully reproduced by the calculated vibrational frequencies, a fact that will become important later in the spectral assignment process.

Table III compares the vibrational frequencies calculated for the $\tilde{X}^2A_1$ state with those obtained for the $\tilde{B}^2A_1$ state of $LiNH_3$ and the $\tilde{X}^1A_1$ state of $LiNH_3^+$. There is good agreement between the CASSCF/MRCI and RCCSD(T)

TABLE II. Vibrational frequencies [a] (in cm^{-1}) of the $\tilde{X}^2A_1$ states of $LiNH_3$ and $LiND_3$.

Vibration	Description [b]	$LiNH_3$ RCCSD(T)/aug-cc-pVTZ	$LiNH_3$ (Matrix IR)[c]	$LiND_3$ RCCSD(T)/aug-cc-pVTZ	$LiND_3$ (Matrix IR)[c]
ν_1 (a_1)	Symm N–H stretch	3408	3278	2438	2372
ν_2 (a_1)	Umbrella	1194	1135	910	882
ν_3 (a_1)	Li–N stretch	439	320	429	(311)
ν_4 (e)	Antisymm N–H stretch	3540	3380	2603	2516
ν_5 (e)	NH_2 scissor	1657	1606	1201	1175
ν_6 (e)	Li–N–H bend	371	381	283	(293)

[a]The experimental data are vibrational fundamental frequencies while the calculated values are unscaled harmonic vibrational frequencies.
[b]These descriptions describe the *approximate* character of the vibrational modes.
[c]From infrared spectra of $LiNH_3$ and $LiND_3$ isolated in an argon matrix (Refs. 3 and 4). The values for $LiND_3$ in parentheses were estimated from a force field analysis (Ref. 4).

TABLE III. Comparison of calculated vibrational frequencies[a] (in cm^{-1}) of the $\tilde{X}^2A_1$ and $\tilde{B}^2A_1$ states of $LiNH_3$ and the $\tilde{X}^1A_1$ state of $LiNH_3^+$.

$LiNH_3$ Vibration	$\tilde{X}^2A_1$ RCCSD(T)	$\tilde{X}^2A_1$ CASSCF + MRCI	$\tilde{B}^2A_1$ CASSCF+ MRCI	$LiNH_3^+$ $\tilde{X}^1A_1$ RCCSD(T)
ν_1 (a_1)	3408	3446	3297	3447
ν_2 (a_1)	1194	1218	1294	1315
ν_3 (a_1)	439	434	560	554
ν_4 (e)	3540	3572	3410	3541
ν_5 (e)	1657	1683	1644	1677
ν_6 (e)	371	384	688	521

vibrational frequencies for the $\tilde{X}^2A_1$ state of $LiNH_3$. The CASSCF/MRCI calculations also yielded vibrational frequencies for the $\tilde{B}^2A_1$ state. Of interest, is the very large increase in the frequency of the Li–N stretching vibration, ν_3, which shifts from 434 to 560 cm^{-1} on excitation from the $\tilde{X}^2A_1$ state of $LiNH_3$ to the $\tilde{B}^2A_1$ state. Indeed the calculated frequency for ν_3 in the $\tilde{B}^2A_1$ state exceeds that in the ground state of the cation, 554 cm^{-1}, a finding that fits with the shorter Li–N bond for the former species discussed earlier.

B. Survey scan for $LiNH_3$

Initial attempts to observe the near-infrared electronic spectrum of $LiNH_3$ were made using photodepletion spectroscopy, as used for other $Li(NH_3)_n$ complexes in our laboratory.[5,7] In the case of $LiNH_3$ this technique involves monitoring the $LiNH_3^+$ ion signal produced by laser photoionization at a wavelength of 283 nm, while scanning the wavelength of the OPO. In order to register IR absorption, this process must induce fragmentation of the neutral, which then leads to a reduction in the monitored $LiNH_3^+$ signal; consequently, IR absorption is registered by dips in this ion signal. UCCSD(T) calculations of the Li–N bond dissociation energy of $LiNH_3$ (4430 cm^{-1})[15] suggest that this energy is easily exceeded by the photon energies used in the present work (see below). Successful observation of a depletion spectrum is also determined by intramolecular decay dynamics, since some of the energy from the initial IR absorption must move into the Li–N stretching vibration, such that Li–N fission can occur on the time scale of the experiment. Since we have electronic excitation of $LiNH_3$, and the dissociation process must take place on the ground state potential energy surface, the rate of internal conversion is critical.

The spectrum in Fig. 1 is a survey scan of $LiNH_3$ obtained in photodepletion mode. This spectrum covers the region from 11300 to 13600 cm^{-1} and consists of several well-resolved bands accompanied by a number of weaker and more congested features on the high frequency side of the spectrum. All of the bands are relatively broad, with full widths at half maximum of approximately 40 cm^{-1}. The linewidth of the OPO is approximately 3 cm^{-1}, so the widths of these bands must be dominated by other factors. We can rule out power broadening, since experiments using reduced OPO pulse energies showed no significant decrease in observed bandwidths. Consequently, the most likely source is lifetime broadening, most probably caused by rapid internal conversion following laser excitation. As a result, no rotational information is obtained from the current work.

One problem with depletion spectroscopy is that laser-induced dissociation of higher mass complexes can sometimes lead to contributions to the ion signal in a particular lower mass channel. For example, depletion of $Li(NH_3)_2$ to produce $LiNH_3$ will ultimately lead to an increase in $LiNH_3^+$ signal on photoionization. This leads to ion signal enhancements which would be seen as structure in the spectrum pointing in the opposite direction to the photodepletion bands seen in Fig. 1. From the low signal levels of the corresponding cations in the mass spectrum, we conclude that $Li(NH_3)_2$ and $Li(NH_3)_3$ are more than an order of magnitude less abundant than $LiNH_3$ in the gas mixture. Furthermore, the absence of any absorption features due to excess ion production, which would produce bands extending below the baseline level in Fig. 1, suggests that cascade effects from larger clusters are negligible. Nevertheless, these observations do not definitively rule out contributions from one or more larger complexes, since there is some possibility, albeit small, of coincident positive- and negative-going signals canceling out each other.

Firm proof that the spectrum arises only from $LiNH_3$ was obtained by recording the two-color REMPI spectrum in

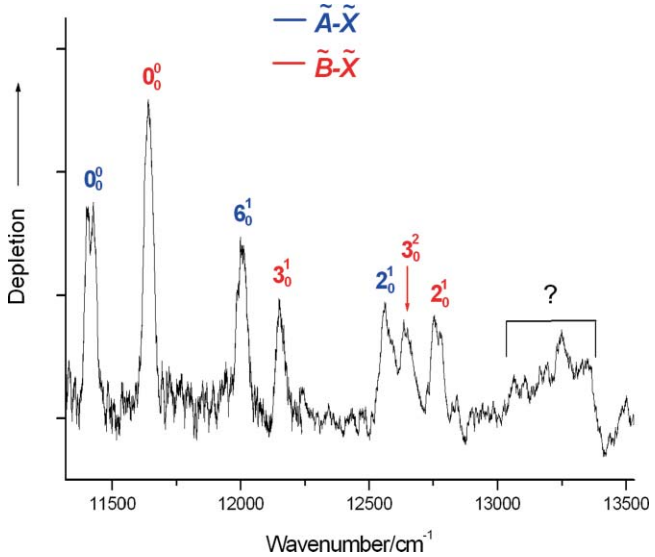

FIG. 1. Electronic spectrum of $LiNH_3$ in the near-infrared obtained using photodepletion spectroscopy. This spectrum was constructed from two separate scans, which are joined at 12250 cm^{-1}. See text for details of the assignment.

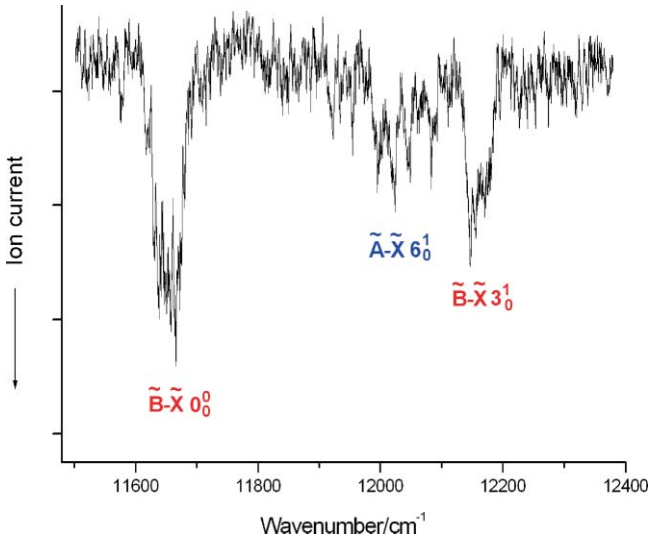

FIG. 2. Part of the two-colour (1+1′) REMPI spectrum of $LiNH_3$ showing the region from 11400 to 12400 cm^{-1}. As detailed in the text, the signal/noise ratio for REMPI spectra was found to be inferior to photodepletion spectra.

the $LiNH_3^+$ mass channel. The wavelength of the frequency doubled dye laser was set at 288 nm introducing a photon with an energy just below the ionization threshold of $LiNH_3$ (4.334 eV or 285.7 nm).[18] When the IR output was added and the wavelength scanned, a REMPI spectrum was observed in which all of the main bands seen for $LiNH_3$ in the photodepletion mode were also obtained in the REMPI spectrum. However, the signal/noise ratio for this spectrum was not as good as that recorded by photodepletion, as can be seen in Fig. 2, which shows part of the REMPI spectrum. The lower quality of the REMPI spectrum presumably arises because the decay of the excited electronic state of $LiNH_3$ is so rapid, which is also consistent with the broad but relatively intense photodepletion bands.

C. Spectral assignments

The positions of the bands observed in the electronic spectra of $LiNH_3$ and $LiND_3$ are summarized in Table IV. To assist with the assignment, we can gain useful clues from previous work, including matrix isolation IR studies of $LiNH_3$, previous work on the electronic spectroscopy of $NaNH_3$, and *ab initio* calculations, including our own.

We will begin by discussing the low frequency part of the spectrum in Fig. 1. We will start with $LiNH_3$ and will then subsequently draw on a comparison with its partially- and fully-deuterated analogues to check the consistency of the assignments made. The band observed at the lowest wavenumber in the spectrum of $LiNH_3$ is at 11423 cm^{-1}. Scans further to the red, extending down to 10500 cm^{-1}, found no other identifiable bands suggesting that this band is likely to be an electronic origin (0_0^0) transition. The $\tilde{A}^2E-\tilde{X}^2A_1$ transition is expected to correlate with the strongly allowed $2p \leftarrow 2s$ transition of atomic lithium. In the free Li atom this transition takes place at 14903 cm^{-1} and so in $LiNH_3$ it is shifted substantially to the red by the presence of the NH_3 group. This parallels the behavior seen previously for $NaNH_3$.[9–12] Assuming C_{3v} point group symmetry for $LiNH_3$, the $\tilde{A}^2E$ state will correlate with the $2p_{x,y}$ orbitals and the $\tilde{B}^2A_1$ state has the Li $2p_z$ orbital as its principal contributor. It is plausible that transitions to both excited electronic states could be observed in our spectra if the states are close enough in energy.

The two lowest frequency vibrations of $LiNH_3$ are, by a large margin, the Li–N stretch (ν_3) and the Li–N–H bend (ν_6). If we assume that the lowest frequency band, at 11 423 cm^{-1}, originates from the $\tilde{A}^2E-\tilde{X}^2A_1$ 0_0^0 transition, then we cannot achieve a sensible band assignment for the three bands immediately above this nominal origin band based on a single electronic transition, even invoking the nontotally symmetric (*e* symmetry) ν_6 bending mode (also known as the rocking mode). This suggests a contribution from two distinct electronic transitions, the $\tilde{A}^2E-\tilde{X}^2A_1$ and $\tilde{B}^2A_1-\tilde{X}^2A_1$ transitions. To gain further information, we also recorded spectra for $LiNH_2D$, $LiNHD_2$, and $LiND_3$. Fig. 3 shows a comparison of the spectra of these isotopologues with that of $LiNH_3$.

We begin our assignment with the aforementioned assumption that the lowest frequency band, at 11423 cm^{-1}, corresponds to the $\tilde{A}^2E-\tilde{X}^2A_1$ 0_0^0 transition. We can then use the isotopic shifts, along with other information, to assign vibrational features in the spectrum. The ratio of frequencies in a given vibrational mode for the nondeuterated versus fully deuterated molecule should be approximately retained from one electronic state to another. Our calculations for the $\tilde{X}^2A_1$ and $\tilde{B}^2A_1$ states confirm this, with the vibrational frequency ratios for the two states agreeing to within 1% for all of the vibrational modes. Consequently, we expect to be able to predict a reliable estimate of this ratio in the $\tilde{A}$ state, even though *ab initio* vibrational frequency calculations on the $\tilde{A}$ state were unsuccessful, by making use of the *ab initio* data for the $\tilde{X}$ state, which has a very similar equilibrium geometry, as noted above. The assignment of the third lowest energy band of $LiNH_3$, at 12035 cm^{-1}, to the 6_0^1 transition, leads to a response to deuteration in line with expectations (experimental ν_6 D/H ratio is 0.79 versus 0.76 from theory). Furthermore, we have carried out additional *ab initio* calculations on the various isotopologues of $LiNH_3$ in its $\tilde{X}$ state, which support this assignment. As can be seen from Table V, the calculations show that the degenerate 6_0^1 band should split into two distinct bands in $LiNH_2D$ (an Li–N–H bend and an Li–N–D bend). Accordingly, we see in the spectra a clear splitting of the

TABLE IV. Band positions[a] and assignments for $LiNH_3$.

$LiNH_3$ band position/cm^{-1}[b]	$LiND_3$ band position/cm^{-1}[b]	Assignment
11423 (0)	11459 (0)	$\tilde{A}-\tilde{X}\ 0_0^0$
11656 (0)	11612 (0)	$\tilde{B}-\tilde{X}\ 0_0^0$
12035 (612)	11940 (481)	$\tilde{A}-\tilde{X}\ 6_0^1$
12162 (506)	12108 (496)	$\tilde{B}-\tilde{X}\ 3_0^1$
12596 (1173)	12342 (883)	$\tilde{A}-\tilde{X}\ 2_0^1$
12676 1020)		$\tilde{B}-\tilde{X}\ 3_0^2$
12808 (1152)	12551 (939)	$\tilde{B}-\tilde{X}\ 2_0^1$

[a]Only bands that have significant signal/noise ratios and are clearly resolved are listed in this table.
[b]The numbers in parentheses show the positions of the bands relative to the respective assigned electronic origin transition.

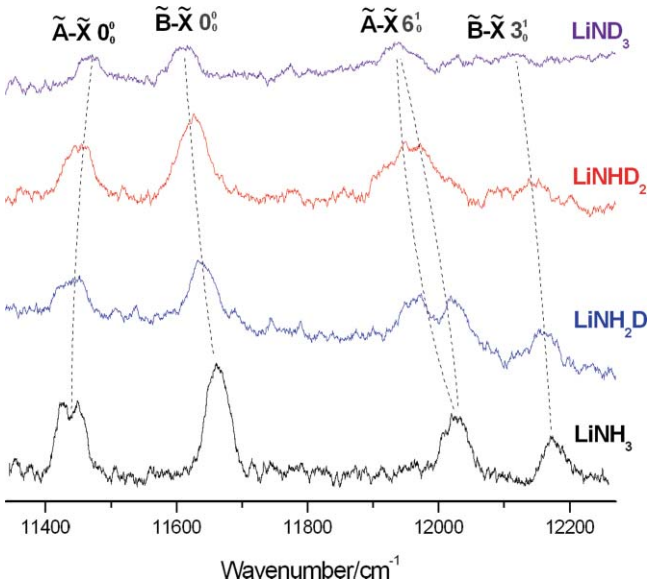

FIG. 3. Comparison of the low frequency regions in the depletion spectra of $LiNH_3$, $LiNH_2D$, $LiNHD_2$, and $LiND_3$. The spectra for the partly and fully deuterated isotopologues were recorded simultaneously by gating the signals for the respective cations in the mass spectrum. A small quantity of ND_3 was injected into the NH_3 flow allowing the H and D atoms to exchange. This results in continuously changing isotopologue ratios as the spectral scan progresses and so these spectra are intended only to show correlations in band positions on isotope substitution: the intensity ratios will not be reliable.

tentatively assigned 6_0^1 feature into two bands, with an approximate separation of 60 cm^{-1}, in going from $LiNH_3$ to $LiNH_2D$ (see Fig. 2). The *ab initio* calculations predict a smaller splitting for $LiNHD_2$ and a significant shift to the red for the two resulting features. In agreement with this prediction we see a clearly broadened, but unresolved, band in Fig. 3 which shows a notable redshift relative to the 6_0^1 band of $LiNH_3$. The bending mode assignment is further confirmed by the additional redshift seen on full deuteration to give $LiND_3$.

Immediately beyond the 6_0^1 band is a second band which is also redshifted on deuteration. The only other low frequency vibration which could possibly be responsible for this band is the ν_3 vibration, where ν_3 is the Li–N stretch. Unlike the 6_0^1 transition, which is nominally forbidden on the basis of simple symmetry arguments, the 3_0^1 transition is symmetrically allowed in the Franck–Condon limit. The absence of any splitting of this band on deuteration is consistent with this vibrational assignment. This band could be assigned to the 3_0^1 transition in the $\tilde{A}^2E - \tilde{X}^2A_1$ system, but this would require a huge increase in the frequency of ν_3, from roughly 440 to 739 cm^{-1}. Not only do the molecular structure changes predicted for the $\tilde{A}^2E - \tilde{X}^2A_1$ transition (see Table I) not support this large change in ν_3 but also a comparison with the corresponding band in $LiND_3$ gives a drastically different ratio of vibrational frequencies (0.87) when compared with the *ab initio* prediction (0.98).

To achieve a sensible assignment, we attribute the bands at 11 656 and 12 035 cm^{-1} to the $\tilde{B}^2A_1 - \tilde{X}^2A_1$ 0_0^0 and 3_0^1 transitions, respectively. Comparison with the corresponding transitions seen for $LiND_3$ now gives a fully deuterated/nondeuterated ν_3 frequency ratio of 0.98, in perfect agreement with the value predicted from *ab initio* calculations. In addition, the frequency extracted for ν_3 in the $\tilde{B}^2A_1$ state of $LiNH_3$, 506 cm^{-1}, is quite close to the MRCI harmonic estimate of 560 cm^{-1} (see Table III).

The conclusions drawn so far, based on the first four bands in the $LiNH_3$ spectrum, are that there are two electronic transitions, the $\tilde{A}^2E-\tilde{X}^2A_1$ and $\tilde{B}^2A_1 - \tilde{X}^2A_1$ transitions, in close proximity. Specifically, we obtain a separation of only 233 cm^{-1} between the two electronic origins. Our CASSCF/MRCI calculations predict a T_e separation of 343 cm^{-1}, which is certainly consistent with the experimental separation given the margins of error that are typical for such excited state transition energy calculations. Previous calculations by Hashimoto and Daigoku using MRCI methodology predicted a separation of *vertical* transitions of around 1200 cm^{-1},[14] which again is reasonably close to the observed separation in view of the likely margin of error in those calculations. Furthermore, Hashimoto and Daigoku predicted almost identical oscillator strengths for the two electronic transitions, which is in accord with the similar band intensities seen in the spectrum in Fig. 1. It is also interesting to note the effect of deuteration on the electronic origin transition energies. For a transition where the binding is stronger in the excited electronic state, deuteration would normally shift the origin of transition to the red. This is indeed the case for the $\tilde{B} - \tilde{X}$ system, where both the ν_3 vibrational assignment and the *ab initio* predictions point to a marked strengthening of the Li–N bond on electronic excitation. Interestingly, the $\tilde{A} - \tilde{X}$ 0_0^0 transition shows a modest blueshift on deuteration. A small blueshift has also been reported previously for the $\tilde{A}^2E-\tilde{X}^2A_1$ 0_0^0 transition of $NaNH_3$ and this was tentatively explained by the suggestion that the binding in the NH_3 entity was weakened by electronic excitation.[10] The *ab initio* calculations carried out in the present work do not provide any specific support for this suggestion in the case of $LiNH_3$, but these calculations were hampered by an inability to calculate vibrational frequencies for the $\tilde{A}^2E$ state.

Having found ν_6 structure in the $\tilde{A}^2E-\tilde{X}^2A_1$ system, we might reasonably look for evidence of excitation of the other low frequency vibration, ν_3. However, we see no additional low frequency features, which would allow such an assignment. The conclusion we draw is that either the ν_3 structure is hidden beneath existing bands, e.g., the 3_0^1 and 6_0^1 bands coincide, or the 3_0^1 band is simply very weak and is

TABLE V. Comparison of the calculated vibrational frequencies of the $\tilde{X}^2A_1$ state of $LiNH_3$ with its partially and fully deuterated analogues[a].

Description [b]	$LiNH_3$	$LiNH_2D$	$LiNHD_2$	$LiND_3$
Li–N–H bend	400 (371)	384 (363)	341 (326)	
Li–N–D bend		320 (306)	297 (283)	295 (283)
Li–N stretch	450 (439)	435 (438)	432 (435)	424 (429)
Umbrella	1223 (1194)	1126 (1103)	1015 (994)	930 (910)
H–N–H bend	1658 (1657)	1616 (1624)		
H–N–D bend		1408 (1417)	1471 (1272)	
D–N–D bend				1274 (1201)

[a]The values not in parentheses are from MP2/6–311++G** calculations, while those in parentheses are from RCCSD(T) calculations using a triple-ζ basis set (see text for details). The harmonic frequencies shown are unscaled. Only those vibrations with frequencies below 2000 cm^{-1}, the region of interest in the current work, are listed here.
[b]These descriptions give the *approximate* character of the vibrational modes.

therefore not observed. The latter suggestion is plausible given the negligible change in the Li–N bond length predicted by the *ab initio* calculations (see Table I), which would confer a small Franck–Condon factor to the 3_0^1 transition.

Likewise, in the $\tilde{B}^2A_1 - \tilde{X}^2A_1$ manifold we have successfully identified structure due to ν_3 but not due to ν_6. However, single quantum excitation of ν_6 is forbidden in the absence of vibronic coupling (see Sec. IV D) and we would not expect any first-order vibronic coupling in the $\tilde{B}^2A_1$ state.

To close this section on band assignments, we turn to the collection of weaker bands in the higher frequency section of the spectra. There is a trio of bands lying between 12 500 and 13 000 cm^{-1} in Fig. 1. An unambiguous assignment for these bands is not possible because more than one plausible transition can contribute. Furthermore, the data from partly and fully deuterated molecules are less definitive for these and higher bands because of their low intensities and the increased congestion. Nevertheless, we have viable suggested assignments which are summarized in Table IV. A totally symmetric vibration that could be active in this region is the NH_3 umbrella mode, ν_2. Bands have been assigned to 2_0^1 in both the $\tilde{A} - \tilde{X}$ and $\tilde{B} - \tilde{X}$ systems for both $LiNH_3$ and $LiND_3$. On the basis of the $\tilde{A} - \tilde{X}$ 2_0^1 assignment, the frequency of ν_2 in the $\tilde{A}$ state is 1173 cm^{-1}, which is close to the calculated ground state value of 1194 cm^{-1} (Table II; RCCSD(T) value). The D/H ratio of vibrational frequencies is 0.75, which is very similar to that expected for the electronic ground state (0.76) based on *ab initio* calculation lending further credence to this assignment. The corresponding ν_2 frequency in the $\tilde{B}$ state is 1152 cm^{-1}, which is significantly below the 1294 cm^{-1} prediction from the CASSCF/MRCI calculations (Table III). Furthermore, the experimental D/H ratio is 0.83 suggesting that the $\tilde{B} - \tilde{X}$ 2_0^1 assignment in $LiNH_3$ or $LiND_3$, or perhaps both, may not be sound.

There are additional, weak, bands above 13 000 cm^{-1}, but there is major congestion in this region and, therefore, specific assignments would be highly speculative. However, we note that several transitions could plausibly lie within this region, including the $\tilde{B} - \tilde{X}$ 3_0^3 band and combination bands such as the $\tilde{A} - \tilde{X}$ $2_0^1 6_0^1$ band.

D. Vibronic coupling

The observation of activity in ν_2 and ν_3 in the spectrum of $LiNH_3$ is not unexpected, since these vibrations are totally symmetric. More surprising is the prominence of the 6_0^1 band in the $\tilde{A}^2E - \tilde{X}^2A_1$ system, since mode ν_6 is nontotally symmetric in the C_{3v} point group and its excitation is therefore symmetry-forbidden at the single quantum level ($\Delta v = \pm 1$) in the Franck–Condon limit, if this point group symmetry is maintained in both electronic states. We note that a prominent 6_0^1 band has also been reported in the corresponding spectrum of $NaNH_3$ and there has been some (unresolved) debate about whether this arises from a Jahn–Teller effect or Herzberg–Teller coupling.[11] Evidence is presented here that shows that Herzberg–Teller coupling dominates in $LiNH_3$.

The Jahn–Teller effect arises from the coupling of vibrational angular momentum with electronic orbital angular momentum within a degenerate electronic state of a nonlinear molecule. When this coupling is significant, the vibrational quantum numbers for Jahn–Teller active vibrations are no longer good quantum numbers, but they can still be used in an approximate sense as a guide to the expected vibrational behavior. In particular, if Jahn–Teller coupling is prominent, we would expect vibrational selection rules for the active vibration(s) of $\Delta v = \pm 0, \pm 1, \pm 2$, etc.[20] In effect, Jahn–Teller distortion converts a nominally nontotally symmetric vibration into a totally symmetric one, in the point group of the distorted structure, subject to the normal Franck–Condon selection rules, and thus a progression in this mode is possible. On the other hand, in Herzberg–Teller coupling, the corresponding vibrational selection rule for the active nontotally symmetric vibration is $\Delta v = \pm 1, \pm 3$, etc.[21] We cannot use these selection rules to distinguish between Herzberg–Teller and Jahn–Teller coupling in $LiNH_3$ since the 6_0^2 and 6_0^3 bands would lie in congested regions of the spectrum where other bands are also clearly present.

However, we have other evidence from the present work which points to a dominant role for Herzberg–Teller coupling. In particular, Herzberg–Teller coupling can persist as the vibrational symmetry is lowered, whereas Jahn–Teller coupling cannot, since all vibrational angular momentum is quenched for $LiNH_2D$ and $LiND_2H$. Consequently, no significant ν_6 structure would be expected for $LiNH_2D$ and $LiND_2H$ if Jahn–Teller coupling was responsible for the 6_0^1 bands seen in the spectra of $LiNH_3$ and $LiND_3$. Furthermore, although the vibrational symmetry is lowered for $LiNH_2D$ and $LiND_2H$, making all vibrational transitions fully allowed in the Franck–Condon limit even without Jahn–Teller or Herzberg–Teller coupling, observable progressions in what were previously nontotally symmetric vibrations would not be expected because there is no change in the equilibrium structure of the molecule on isotopic substitution. Since we observe the 6_0^1 band just as readily for $LiNH_2D$ and $LiND_2H$ as we do for $LiNH_3$ and $LiND_3$, we therefore conclude that Herzberg–Teller coupling is responsible for the appearance of the nominally forbidden 6_0^1 band.

The prominence of this band must derive from substantial intensity borrowing from one or more electronically allowed transitions. The vibrational wavefunction for the $\nu_6 = 1$ level in $LiNH_3$ has e symmetry and can potentially mix with the wavefunction of the $\tilde{A}^2E$ state to give *vibronic* states with A_1 and E symmetries. An A_1 vibronic state would now have the correct symmetry to interact with other electronic states of A_1 symmetry and in particular the nearby $\tilde{B}^2A_1$ state. According to the *ab initio* predictions by Hashimoto and Daigoku the $\tilde{B}^2A_1 - \tilde{X}^2A_1$ electronic transition has virtually the same oscillator strength as the $\tilde{A}^2E - \tilde{X}^2A_1$ transition.[14] Consequently, the "borrowing" of substantial intensity from the $\tilde{B}^2A_1 - \tilde{X}^2A_1$ transition is a plausible source of the strong vibronically-allowed 6_0^1 band seen in the $\tilde{A}^2E - \tilde{X}^2A_1$ system of $LiNH_3$.

V. CONCLUSIONS

The electronic spectrum of the prototypical alkali-ammonia complex, $LiNH_3$, has been recorded for the first

time. This spectrum, occurring in the near-infrared, shows bands assigned to both the $\tilde{A}^2E$ -$\tilde{X}^2A_1$ and $\tilde{B}^2A_1 - \tilde{X}^2A_1$ electronic transitions. In particular the origin bands for these two transitions are found to be in very close proximity ($\sim$200 cm^{-1}). Vibrational structure in these two band systems has been identified and assigned with the aid of isotope substitution studies and a series of supporting *ab initio* calculations.

The $\tilde{A}^2E - \tilde{X}^2A_1$ system is characterized by prominent activity of the Li–N–H bending vibration (ν_6) implying strong vibronic coupling in the excited electronic state. Jahn–Teller activity is possible in the $\tilde{A}^2E$ state, which could give rise to observation of Franck–Condon-forbidden features, such as the intense 6_0^1 band. However, evidence from isotope substitution experiments suggests that the vibronic activity is a consequence of Herzberg–Teller coupling. In particular, the proximity of the $\tilde{B}^2A_1$ state to the $\tilde{A}^2E$ state provides the opportunity for strong vibronic coupling.

ACKNOWLEDGMENTS

The authors would like to thank the UK Engineering and Physical Sciences Research Council (EPSRC) for a grant in support of this work. Computational aspects were supported through the EPSRC National Service for Computational Chemistry, which provided both software and hardware resources and from both the University of Leicester Mathematical Modeling Centre and the University of Nottingham HPC facility. A departmental contribution toward the studentship of L.V. is also gratefully acknowledged.

[1] J. C. Thompson, *Electrons in Liquid Ammonia* (Clarendon, Oxford, 1976).
[2] E. Zurek, P. P. Edwards, and R. Hoffmann, Angew. Chemie Int. Ed. **48** 8198 (2009).
[3] S. Suzer and L. Andrews, J. Am. Chem. Soc. **109**, 300 (1987).
[4] A. Loutellier, L. Manceron, and J. P. Perchard, Chem. Phys. **146**, 179 (1990).
[5] T. E. Salter, V. A. Mikhailov, C. J. Evans, and A. M. Ellis, J. Chem. Phys. **125**, 034302 (2006).
[6] T. E. Salter, V. Mikhailov, and A. M. Ellis, J. Phys. Chem. A **111**, 8344 (2007).
[7] L. Varriale, N. M. Tonge, N. Bhalla, and A. M. Ellis, J. Chem. Phys. **132**, 161101 (2010).
[8] W. S. Hopkins, A. P. Woodham, N. M. Tonge, A. M. Ellis, and S. R. Mackenzie, J. Phys. Chem. Lett. **2**, 257 (2011).
[9] C. Nitsch, C. Huglin, I. V. Hertel, and C. P. Schulz, J. Chem. Phys. **101**, 6559 (1994).
[10] C. P. Schulz and C. Nitsch, J. Chem. Phys. **107**, 9794 (1997).
[11] D. A. Rodham and G. A. Blake, Chem. Phys. Lett. **264**, 522 (1997).
[12] P. Brockhaus, I. V. Hertel, and C. P. Schulz, J. Chem. Phys. **110**, 393 (1999).
[13] K. Hashimoto and K. Daigoku, Chem. Phys. Lett. **469**, 62 (2009).
[14] K. Hashimoto and K. Daigoku, Phys. Chem. Chem. Phys. **11**, 9391 (2009).
[15] T. E. Salter and A. M. Ellis, Chem. Phys. **332**, 132 (2007).
[16] *Gaussian 03, Revision C.02*, M. J. Frisch, G. W. Trucks, H. B. Schlegel *et al.*, GAUSSIAN 03, *Revision C.02*, Gaussian, Inc., Wallingford CT, 2004.
[17] MOLPRO, a package of *ab initio* programs written by H.-J. Werner and P. J. Knowles with contributions from J. Almlöf, R. D. Amos, A. Berning *et al.*
[18] T. E. Salter and A. M. Ellis, J. Phys. Chem. A **111**, 4922 (2007).
[19] R. Wieczorek, P. Durlak, and Z. Latajka, Polish J. Chem. **83**, 761 (2009).
[20] M. Heaven, T. Sears, V. E. Bondybey, and T. A. Miller, J. Chem. Phys. **75**, 5271 (1981).
[21] P. Bernath, *Spectra of Atoms and Molecules* (Oxford University Press, New York, 2005).